OPEN ACCESS

Decoupling Failure Pathways in Li-O_2 Cells Operated Under Lean Electrolyte Conditions

To cite this article: Daniel Córdoba *et al* 2025 *J. Electrochem. Soc.* **172** 110530

Journal of The Electrochemical Society, 2025 **172** 110530

Decoupling Failure Pathways in Li-O_2 Cells Operated Under Lean Electrolyte Conditions

Daniel Córdoba,[1,2] Matthew Li,[1,z] Xiaozhou Huang,[1] Yanan Gao,[1,3] Shoichi Matsuda,[1,3] Ernesto J. Calvo,[2,*,z] and Khalil Amine[1,z]

[1]*Chemical Sciences and Engineering Division, Argonne National Laboratory, Lemont, Illinois 60439, United States of America*
[2]*INQUIMAE (CONICET-UBA), Facultad de Ciencias Exactas y Naturales - Universidad de Buenos Aires, Ciudad Universitaria, Ciudad Autónoma de Buenos Aires, Argentina*
[3]*Center for Green Research on Energy and Environmental Materials, National Institute for Materials Science, Tsukuba, Ibaraki 305-0044, Japan*

The operation of lithium-oxygen (Li-O_2) batteries under lean electrolyte conditions offers higher energy density but leads to rapid degradation and short cycle life. Although cathode passivation and electrolyte decomposition occur in all regimes, we show that under lean electrolyte conditions, failure is primarily driven by progressive electrolyte consumption at the lithium/solid electrolyte interphase (SEI), rather than by irreversible cathode passivation. Poor wetting of the lithium surface results in heterogeneous SEI growth and high local current densities, which accelerate electrolyte loss and cell failure. Strategies aimed at improving interfacial stability, including optimized wetting and SEI forming additives, significantly extend cycle life without compromising energy density. Our results establish anode-electrolyte interactions as the dominant degradation mechanism under lean electrolyte conditions, and emphasize the need to engineer a stable Li/SEI interface for long-lasting Li-O_2 batteries.
 [DOI: 10.1149/1945-7111/ae1ea5]

Manuscript submitted August 12, 2025; revised manuscript received October 25, 2025. Published November 21, 2025.

Supplementary material for this article is available online

Lithium-oxygen batteries (LOBs) are considered one of the most promising next-generation energy storage systems due to their high theoretical energy density.[1] However, their practical implementation is severely limited by large charge overpotentials, parasitic reactions, electrolyte instability, and rapid capacity fade during cycling.[2–4] One of the most straightforward strategies to maximize the gravimetric energy density is to minimize the amount of electrolyte, operating under so-called "lean electrolyte" conditions.[5] While this strategy enables higher cell-level energy density, it is consistently associated with a drastic reduction in cycle life and accelerated degradation compared to cells flooded with excess electrolyte.[6]

Matsuda and collaborators[7–11] have made key contributions to the study of LOBs under lean electrolyte conditions. In one of their works, they identified that the accumulation of byproducts represents a relevant failure mechanism; since these byproducts do not easily dissipate, they form passivating layers that block oxygen channels and lead to premature cell death. In another study, they showed that contaminants such as H_2O and CO_2, originating from the cathode, reduce lithium electrode efficiency and accelerate its degradation. They also demonstrated that irreversible volume changes in the electrodes, together with electrolyte redistribution in the cathode, intensify the deterioration of these cells. Finally, they revealed that when lean electrolyte and high capacity are combined, carbon decomposition above 3.8 V becomes the key factor that shortens cell lifespan.

In our previous work,[12] we systematically compared LOBs cycled under electrolyte-limited conditions (10 $\mu l\ cm^{-2}$) and flooded conditions (100 $\mu l\ cm^{-2}$). We demonstrated that the cathode side remains largely unaffected by the electrolyte volume: the Li_2O_2 discharge product retains the same crystalline morphology, with similar yield (~74%–77%), without a significant increase in singlet oxygen ($^1O_2$) formation or parasitic oxygen evolution reactions. Zor et al.[13] investigated the stability of tetraethylene glycol dimethyl ether (G4) against $^1O_2$ and concluded that its contribution to chemical degradation during discharge is practically negligible, accounting for only 0.002% of the total.

In addition, differential electrochemical mass spectrometry (DEMS) confirmed that the overall oxygen evolution reaction (OER) efficiency is comparable under both conditions. Similarly, X-ray photoelectron spectroscopy (XPS) revealed that the chemical composition of the solid-electrolyte interphase (SEI) on the lithium anode does not vary significantly between lean and flooded conditions.[12]

Despite these similarities, electrolyte-limited cells exhibit much faster degradation, accelerated impedance growth, and premature failure.[6,12,14] Post-mortem analysis revealed that the SEI morphology differs markedly under lean conditions, where the electrolyte wets the surface non-uniformly, leaving areas of lithium exposed. This creates regions of high local current density, leading to the formation of a thick, porous outer SEI layer with high diffusional resistance and, ultimately, severe electrolyte consumption.[6,15] These observations suggest that the failure mechanism under electrolyte-limited conditions is dominated by electrolyte drying and unstable anode wetting rather than intrinsic cathode degradation.

Building on these conclusions, in the present work we aim to directly track the failure pathway of Li-O_2 cells operated under electrolyte-limited conditions. We combine controlled cycling experiments, electrode reassembly tests, and cell design modifications (vacuum wetting, uniform pressure distribution, and anode-protective additives) to determine whether failure originates from irreversible electrode passivation or from electrolyte depletion. Under conditions of lean electrolyte, the rapid degradation of LOBs is mainly driven by insufficient wetting of the lithium anode, which leads to gradual electrolyte depletion at the Li/SEI interface.

Experimental

Cell assembly.—A 10 mm diameter and 200 μm thick lithium metal disc was used as the anode, while a Celgard 2500 (25 μm thickness) separator was impregnated with different volumes of electrolyte. A commercial 10 mm diameter carbon gas diffusion layer from MTI Corporation (EQ-bcgdl-1400S-LD) was dried at 120 °C under vacuum overnight and used as the cathode, and a 316 stainless-steel mesh was used as the current collector.

The electrolyte consisted of 1 M lithium bis(trifluoromethanesulfonyl)imide (LiTFSI) dissolved in tetraethylene glycol dimethyl

*Electrochemical Society Fellow.
[z]E-mail: matthew.li@anl.gov; ernestojulio.calvo@gmail.com; amine@anl.gov

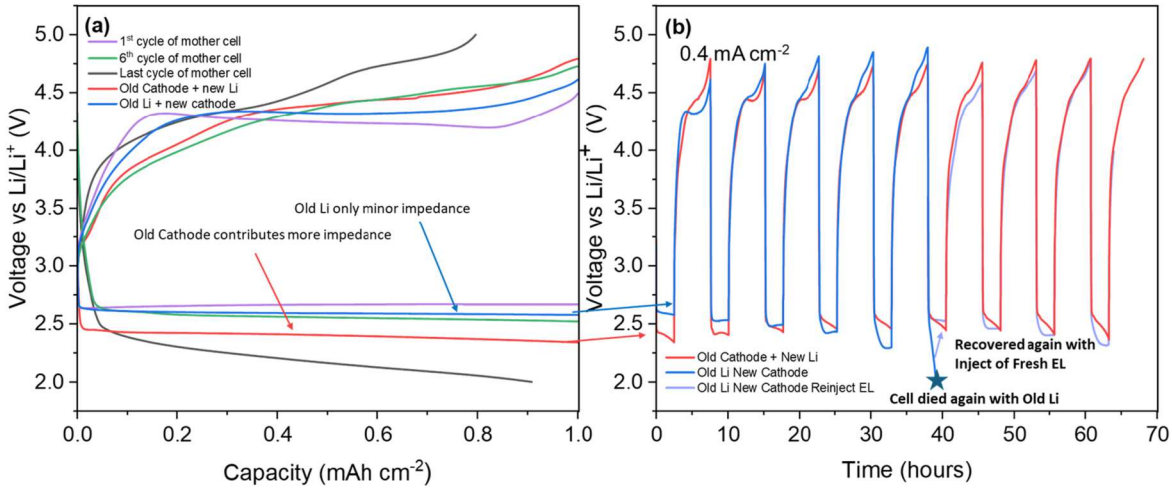

Figure 1. (a) Voltage-capacity profiles of the cell operated under lean electrolyte conditions for cycles 1, 6, and the final cycle of the "mother" cell, as well as for electrodes collected and reassembled with new counterparts: old cathode + new lithium and old lithium + new cathode. (b) Cycling stability of the newly reassembled cells with aged electrodes and their new counterparts; the blue star indicates the point of fresh electrolyte reinjection for the old lithium + new cathode cell.

ether (G4). For the lithium nitrate ($LiNO_3$) containing cells, 0.2 M was added as an additive. Both LiTFSI and $LiNO_3$ was dried in vacuum oven at 120 °C overnight and G4 was dried over molecular sieve for 3 days before use.

The batteries were assembled using Swagelok-type cell, to ensure consistent electrolyte distribution, 2.5 μl of electrolyte were first dispensed onto the Li surface before placing the separator, followed by 7.5 μl onto the cathode prior to cell closure. Once assembled, the cells were placed into a ∼50 ml vessel, removed from the glovebox, purged with oxygen at a pressure of 1 bar for 15 min, and then left to rest for 2 h before starting the electrochemical tests. The large volume of the enclosure mitigates the impact of oxygen partial pressure on the performance.

Electrochemical characterization.—Galvanostatic discharge-charge experiments were performed on a Neware cycler with the selected current density and capacity limits as described in the experimental results. Electrochemical surface area (ECSA) was measured by performing cyclic voltammetry of Swagelok cells under Ar atmosphere across ±100 mV vs OCV at scan rates of 0.05 to 1 mV s^{-1} (shown in Fig. S1). The current densities values at the potential end points (100 mV and −100 mV vs OCV) were subtracted and divided by two to obtain the current density for fitting the slope. Electrochemical impedance spectroscopy (EIS) was performed using Swagelok cells under identical experimental conditions, with a frequency range of 0.1 Hz to 1000 kHz and a voltage amplitude of 10 mV on a Solartron.

Stack pressure optimization: Improved pressure uniformity was achieved by employing multiple springs in parallel (nested) to achieve better contact with the lithium metal. Fuji Prescale pressure-sensitive film was used to confirm the improved uniformity of the stack pressure, as shown in Fig. S2. Vaccum wetting was performed as follows: after cell fabrications and electrolyte injection by drop casting onto the Li and cathodes. The cell stack was placed into a vacuum oven at room temperature and held at ∼0.2 atm for 30 s and then refilled to 1 atm. This was performed twice. The typical wetting technique included just simply injecting the electrolyte with a pipette without any vacuum.

Results and Discussion

Identifying the origin of failure under lean electrolyte conditions.—To understand the mechanism of accelerated degradation under electrolyte-limited conditions, we first evaluated whether the capacity loss is associated with irreversible damage to the cathode or the anode. Selective electrode reassembly experiments were designed, reusing aged cathodes and anodes in new configurations paired with fresh counterparts. This approach allows decoupling the contribution of each electrode to the failure pathway and distinguishing whether premature cell death is caused by irreversible passivation or by phenomena related to electrolyte consumption or distribution.

Figure 1a shows the voltage-capacity profiles of a cell operated under lean electrolyte conditions, highlighting cycles 1 (purple), 6 (green), and the final cycle 12 (black) of the mother cell. A progressive increase in the charge overpotential is observed with continued cycling.

After cell failure, the electrodes were recovered, rinsed with 1,2 dimethoxymethane, dried, and reassembled into new cells containing fresh electrolyte and pristine counterparts. The cell employing the aged cathode with new lithium (red curve) exhibited extended cycling stability, whereas the one using the aged lithium anode failed rapidly (blue curve), as shown in Fig. 1b. Upon electrolyte reinjection (marked with a blue star) capacity was restored, confirming that cell failure originated from electrolyte depletion at the anode rather than from irreversible cathode passivation. Although the aged cathode introduced a moderate increase in charge overpotential, likely due to slight surface passivation,[16] it did not substantially limit the capacity.

These observations indicate that, while cathode passivation contributes to impedance build-up, cell death occurs only when electrolyte loss at the anode disrupts ionic percolation, as evidenced by the capacity recovery upon electrolyte replenishment. The increased impedance (manifested as the higher overpotential in the "old Li + new cathode" trace of Fig. 1b) stems from the formation of a porous SEI on the lithium surface.

Similar electrolyte-refiling strategies have been explored in previous studies as an effective way to mitigate the adverse effects associated with electrolyte loss or degradation during aging. Kuzovchikov et al.[17] demonstrated that electrolyte refilling in aged pouch cells significantly restores capacity, even at advanced states of health, by reducing internal impedance and improving ionic contact. Complementary studies on artificially dried 18650 cylindrical cells showed that electrolyte replenishment helps prevent abrupt capacity fade (rollover failure) and restores the original electrochemical performance.[18,19]

Overall, these results demonstrate that cell failure under lean electrolyte operation does not originate from irreversible lithium metal degradation but from progressive electrolyte depletion, promoted by poor anode wetting and the development of a porous SEI.[6,12,20]

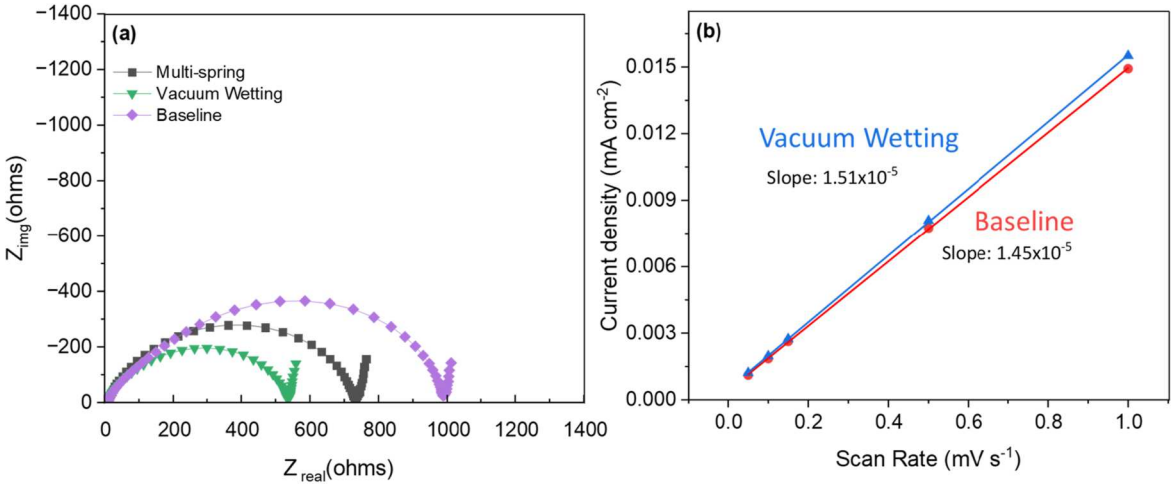

Figure 2. (a) Nyquist plots under an argon atmosphere for cells without modifications (baseline), multi-spring, and vacuum wetting. (b) Electrochemically active area obtained from capacitive currents as a function of scan rate for baseline and vacuum wetting.

Strategies to improve the initial wetting of the anode.—Since the reassembly experiments indicated that failure is dominated by the instability of the Li/SEI interface, physical strategies were explored to improve the initial wetting of the anode and minimize the formation of dry spots.[21] In particular, a vacuum wetting technique was implemented to optimize electrolyte distribution during cell assembly, and a multi-spring design applying controlled pressure was evaluated to maintain more uniform contact between the cell components. The effectiveness of these strategies was analysed using impedance spectroscopy, electrochemical surface area measurements and cycling tests.

Figure 2a shows the Nyquist plots under an argon atmosphere for three full cells: the cell without initial modifications (baseline, purple dots), vacuum wetting (green), and multi-spring (black). The impedance was monitored as a function of time to determine whether diffusion-controlled growth that is characteristic of SEI growth exist.[22] Figure S3 indeed shows at a clear linear trend of impedance (baseline cell) vs $t^{0.5}$ suggesting that this impedance is majorly contributed by SEI which can only occur at the lithium anode. The baseline cell exhibits the largest semicircle, indicating higher interfacial resistance. The cell with vacuum wetting shows a smaller semicircle, reflecting better initial contact and lower impedance at the lithium anode. The multi-spring design presents an intermediate behaviour.

Figure 2b shows the calculation of the electrochemically active surface area from capacitive currents. The slope is practically identical (~4% difference) for both the baseline and vacuum wetting, resulting in similar values of ECSA. This confirms that vacuum wetting does not significantly modify the active surface of the cathode but rather improves the wetting of the anode, reducing the initial resistance. Although vacuum wetting reduces the initial resistance and minimizes dry areas at the beginning, its impact on cycle life is limited.

Figure 3 shows the voltage evolution as a function of time for the different cell configurations. The first five cycles were performed at a current density of 0.2 mA cm^{-2}, while the subsequent cycles were discharged at the same current density but charged at 0.4 mA cm^{-2}. Vacuum wetting (blue line) maintains stable voltages for 16 cycles, the multi-spring (green) reaches 14 cycles, and the baseline cell (red) fails after 11 cycles. A capacity below 0.5 mAh cm^{-2} was used as the failure criterion. Although a modest improvement is observed with vacuum wetting, the fundamental degradation mechanism is not eliminated, as the electrolyte continues to be consumed at the Li/SEI interface, limiting the cycle life.[15]

Analysis of electrolyte oxidation and its relation to cycle life.—While cell degradation is primarily attributed to the progressive consumption of the electrolyte at the anode, the direct oxidation of the solvent above 4.7 V vs Li/Li$^+$ cannot be ruled out. Although potentials above 4.0 V may trigger minor oxidative side reactions, this range was intentionally maintained to capture realistic failure onset and morphology changes associated with lean operation. A blank-cell test (Fig. S4) confirms that G4 oxidation remains limited up to approximately 4.7 V under these conditions.

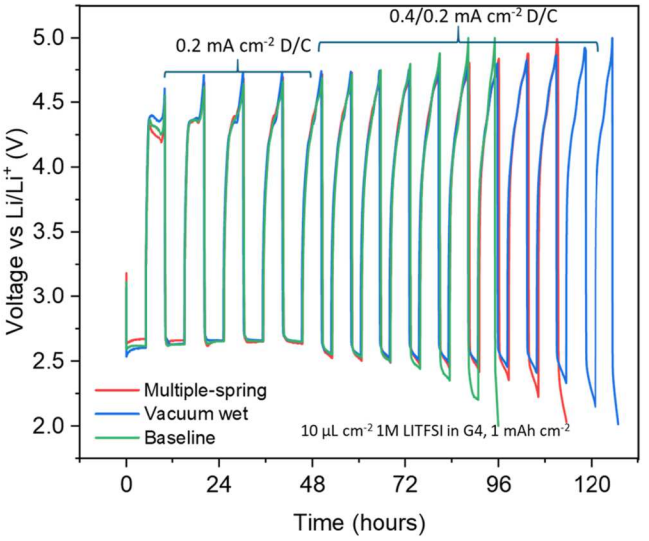

Figure 3. Voltage evolution as a function of time for cells without modifications (baseline), multi-spring, and vacuum wetting, at different current densities.

Figure 4a shows the capacity associated with the direct oxidation of the G4 solvent above 4.7 V vs Li/Li$^+$ as a function of cycle number. An increase in this oxidation is observed in the final cycles before failure. Vacuum wetting exhibits higher early oxidation compared to the baseline and multi-spring configurations. Figure 4b presents the accumulated capacity above 4.7 V vs Li/Li$^+$. Under all conditions, this value increases progressively, but without a clear threshold marking failure.

The slightly higher early oxidation observed for vacuum-wetted cells may result from deeper electrolyte infiltration penetration into the porous cathode, which temporarily increases the effective electrochemical surface area without compromising overall cell stability. No distinct capacity threshold above 4.7 V was identified that could predict failure, further ruling out solvent oxidation runaway as the dominant degradation pathway under these conditions.

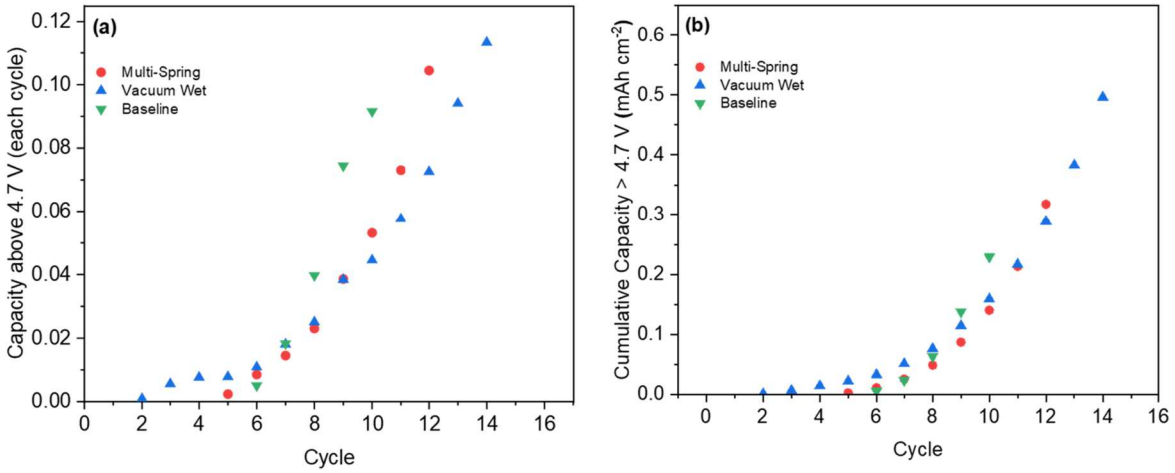

Figure 4. (a) Capacity associated with the direct oxidation of the G4 solvent above 4.7 V as a function of cycle number for baseline, multi-spring, and vacuum wetting. (b) Cumulative capacity above 4.7 V vs Li/Li$^+$ as a function of cycle number for the same conditions.

Therefore, although G4 oxidation does occur above 4.7 V, it does not dictate cell failure. The cell ultimately fails independently of the accumulated extent of solvent oxidation, confirming that the prevailing degradation mechanism is the progressive electrolyte consumption at the anode rather than irreversible cathode passivation.

Mitigation of degradation via anode-protecting additives.— Finally, we explored a strategy based on the *in situ* engineering of the Li/SEI interface through the addition of an anode-protecting electrolyte additive during cycling. Ideally, SEI layers formed in this way exhibit suitable mechanical integrity and lithium-ion conductivity, helping to reduce electrolyte loss and improve anode stability under lean electrolyte conditions.[20] This approach was tested as an alternative to previously presented physical optimizations, with the aim of extending the cycle life without compromising energy density.

Lithium nitrate has been proposed as a as a promising additive for LOBs due to its ability to stabilize the lithium anode through SEI formation, its low degree of dissociation in aprotic solvents, and its catalytic effect on the oxygen evolution reaction.[23] To promote the formation of a more stable SEI and supress electrolyte consumption at the Li interface, we incorporated 0.2 M of $LiNO_3$ into a 1 M LiTFSI in G4 electrolyte.

Figure 5 shows the evolution of specific capacity with cycle number under lean electrolyte conditions. The baseline cell failed after 11 cycles, while cells assembled using vacuum wetting and the multi-spring configuration exhibited moderate improvements, reaching 14 and 16 cycles, respectively. In contrast, the cell containing $LiNO_3$ maintained stable performance for up to 29 cycles.

The corresponding voltage profiles (Fig. S5) further confirm the dual functionality of $LiNO_3$ as both an SEI-stabilizing additive and a partial redox mediator.[23] During cycling, NO_3^- ions are reduced at the anode to form NO_2^-, which can subsequently oxidize to NO_2, thereby facilitating Li_2O_2 oxidation.[24] Moreover, $LiNO_3$ affects the morphology of the deposited Li_2O_2, which influences cathode passivation and contributes to the overall cell behaviour.[25]

While the additive nearly triples the cell lifespan, it does not significantly shift the abrupt capacity drop ($\sim$1 mAh cm^{-2}). Instead, it induces a more gradual rollover, suggesting that although the dominant degradation mechanism remains electrolyte consumption at the Li/SEI interface, it is mitigated by the formation of a denser and more stable SEI. In addition, the redox-mediating action of nitrate-derived species facilitates Li_2O_2 oxidation at the cathode, improving reversibility and delaying passivation. Together, these effects account for the extended cycle life and smoother capacity decay observed in $LiNO_3$ containing cells.

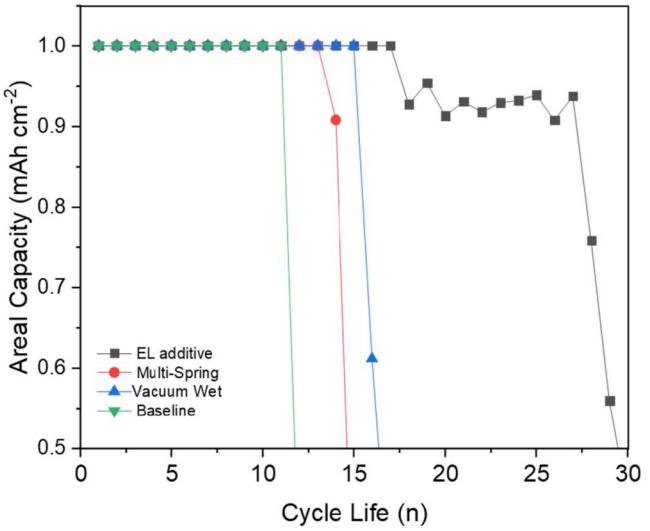

Figure 5. Specific capacity vs cycle number for Li-O_2 cells under lean electrolyte conditions, comparing baseline, vacuum wetting, multi-spring, and the addition of 0.2 M of $LiNO_3$ in 1 M LiTFSI/G4. The first five cycles were carried out at 0.2 mA cm^{-2}, followed by cycles at 0.4 mA cm^{-2}.

Conclusions

While both cathode passivation and electrolyte degradation contribute to performance fading in Li-O_2 cells, our results reveal that, under lean electrolyte conditions, the dominant failure mechanism shifts toward electrolyte depletion at the lithium/SEI interface. In this regime, insufficient wetting of the lithium surface promotes heterogeneous SEI growth and localized electrolyte consumption, ultimately accelerating impedance rise, capacity loss, and cell failure.

Selective electrode reuse experiments confirm that the cathode does not undergo irreversible passivation under the electrolyte filling and cycling conditions employed, whereas the aged lithium anode is the limiting component responsible for premature failure.

Physical strategies designed to improve initial wetting, such as vacuum wetting and uniform pressure distribution through multi-spring configurations effectively reduce interfacial resistance and delay degradation, but they do not eliminate the fundamental cause of failure, which remains progressive electrolyte depletion at the Li/SEI interface.

In contrast, incorporating SEI-forming additives such as $LiNO_3$ markedly extends the cycle life. This improvement arises from the formation of a denser, less permeable SEI that mitigates electrolyte loss, together with the redox-mediating behaviour of nitrate-derived species that facilitate Li_2O_2 oxidation and delay cathode passivation. Nevertheless, the additive does not alter the ultimate capacity drop threshold, indicating that while the degradation pathway is moderated, the governing mechanism remains electrolyte consumption.

Complementary analysis of G4 solvent oxidation above 4.7 V vs Li/Li^+ reveals that although oxidative reactions accumulate with cycling, no abrupt onset of solvent breakdown is detected. This rules out oxidative runaway as the primary degradation mode and reinforces that electrolyte loss at the anode dominates failure.

Taken together, these results establish that stabilizing the Li/SEI interface either through improved wetting, optimized pressure control, or SEI-forming/mediating additives is critical to extending the operational life of Li-O_2 batteries under electrolyte-limited conditions. Engineering this interface provides a practical path toward longer-lasting, high-energy Li-O_2 systems without compromising gravimetric energy density.

Acknowledgments

The authors gratefully acknowledge support of this work from the U.S. Department of Energy (DOE), Office of Energy Efficiency and Renewable Energy, Vehicle Technologies Office. Argonne National Laboratory is operated for the U.S. DOE, Office of Science, by UChicago Argonne, LLC, under Contract No. DE-AC02–06CH11357. D.C acknowledges support from a postdoctoral research fellowship awarded by the National Scientific and Technical Research Council (CONICET), Argentina. E.J.C. is a fellow member of CONICET, Argentina. Y.G. and S.M. acknowledge support by Japan Science and Technology Agency (JST), Adopting Sustainable Partnerships for Innovative Research Ecosystem (ASPIRE), under Contract No. JPMJAP2309.

ORCID

Daniel Córdoba https://orcid.org/0000-0001-6823-9972
Matthew Li https://orcid.org/0000-0001-9093-3207
Xiaozhou Huang https://orcid.org/0000-0002-7660-0382
Yanan Gao https://orcid.org/0000-0003-0217-6512
Shoichi Matsuda https://orcid.org/0000-0002-0640-3404
Ernesto J. Calvo https://orcid.org/0000-0003-0397-2406
Khalil Amine https://orcid.org/0000-0001-9206-3719

References

1. P. G. Bruce, S. A. Freunberger, L. J. Hardwick, and J.-M. Tarascon, *Nat. Mater.*, **11**, 19 (2012).
2. A. C. Luntz and B. D. McCloskey, *Chem. Rev.*, **114**, 11721 (2014).
3. W.-J. Kwak et al., *Chem. Rev.*, **120**, 6626 (2020).
4. H. Xiaozhou, L. Matthew, and A. Khalil, *Renewables*, **2**, 421 (2024).
5. S. Matsuda, *Electrochemistry*, **91**, 101006 (2023).
6. H. Kwon, J. Baek, and H.-T. Kim, *Energy Storage Mater.*, **55**, 708 (2023), https://sciencedirect.com/science/article/pii/S2405829722006730.
7. S. Matsuda et al., *Adv. Energy Mater.*, **13**, 2203062 (2023).
8. S. Matsuda, S. Kimura, and K. Uosaki, *The Journal of Physical Chemistry C*, **127**, 11822 (2023).
9. M. Ono, J. Saengkaew, and S. Matsuda, *Adv. Sci.*, **10**, 2300896 (2023).
10. S. Matsuda et al., *ACS Appl. Energy Mater.*, **4**, 2563 (2021).
11. S. Matsuda and H. Asahina, *The Journal of Physical Chemistry C*, **124**, 25784 (2020).
12. D. Córdoba et al., *The Journal of Physical Chemistry C*, **129**, 3404 (2025).
13. C. Zor et al., *Energy Environ. Sci.*, **17**, 7355 (2024).
14. S. C. Nagpure et al., *J. Power Sources*, **407**, 53 (2018), https://sciencedirect.com/science/article/pii/S0378775318311686.
15. H. Li et al., *J. Am. Chem. Soc.*, **142**, 2012 (2020).
16. P. Albertus et al., *J. Electrochem. Soc.*, **158**, A343 (2011).
17. S. M. Kuzovchikov et al., *J. Power Sources*, **601**, 234257 (2024), https://sciencedirect.com/science/article/pii/S0378775324002088.
18. F. Arshad et al., *ACS Sustain Chem Eng*, **8**, 13527 (2020).
19. X. Lai et al., *J Energy Storage*, **52**, 104951 (2022), https://sciencedirect.com/science/article/pii/S2352152X22009574.
20. M. G. Nam, S. W. Jeong, and P. J. Yoo, *Adv. Energy Mater.*, **15**, 2400035 (2025).
21. F. Chen et al., *Green Energy and Intelligent Transportation*, **4**, 100248 (2025), https://sciencedirect.com/science/article/pii/S2773153724001002.
22. C. D. Alt et al., *Joule*, **8**, 2755 (2024), https://sciencedirect.com/science/article/pii/S2542435124003350.
23. Rosy, S. Akabayov, M. Leskes, and M. Noked, *ACS Appl. Mater. Interfaces*, **10**, 29622 (2018).
24. D. Sharon et al., *ACS Appl. Mater. Interfaces*, **7**, 16590 (2015).
25. C. M. Burke, V. Pande, A. Khetan, V. Viswanathan, and B. D. McCloskey, *Proc. Natl Acad. Sci.*, **112**, 9293 (2015).